

## Field tests and multiphysics analysis of a flooded shaft for geothermal applications with mine water



Ting Bao<sup>a</sup>, Zhen Liu<sup>b,\*</sup>, Jay Meldrum<sup>c</sup>, Christopher Green<sup>d</sup>, Pengfei Xue<sup>e</sup>, Stanley Vitton<sup>f</sup>

<sup>a</sup> Department of Civil and Environmental Engineering, Michigan Technological University, 1400 Townsend Drive, Dow 854, Houghton, MI 49931, United States

<sup>b</sup> Department of Civil and Environmental Engineering, Michigan Technological University, 1400 Townsend Drive, Dillman 201F, Houghton, MI 49931, United States

<sup>c</sup> Keweenaw Research Center, Michigan Technological University, 23620 Airpark Boulevard, Calumet, MI 49931, United States

<sup>d</sup> Senior Research Engineer, Keweenaw Research Center, Michigan Technological University, 23620 Airpark Boulevard, Calumet, MI 49931, United States

<sup>e</sup> Department of Civil and Environmental Engineering, Michigan Technological University, 1400 Townsend Drive, GLRC 317, Houghton, MI 49931, United States

<sup>f</sup> Department of Civil and Environmental Engineering, Michigan Technological University, 1400 Townsend Drive, Dillman 201G, Houghton, MI 49931, United States

### ARTICLE INFO

#### Keywords:

Geothermal energy  
Mine water  
Thermo-hydrodynamic process  
Buoyancy-driven flow  
Upper Peninsula

### ABSTRACT

This paper introduces the scientific part of a large-scale study in the Upper Peninsula (U.P.) of Michigan, a historical mining area, for exploring the water in deep abandoned copper mines as a geothermal energy resource. The main focus of the paper is placed on the scientific understanding of the natural mine water-geologic formation system, especially the transport of heat and mass in this large-scale natural system, which is critical to the efficiency and sustainability of the energy renovation. For this purpose, a field study involving measurements of temperatures and chemicals in a local mine shaft in the U.P. is conducted to reveal the major issue in recovering geothermal energy in the water from the shaft, i.e., the temperature distribution. Water samples are also collected in situ to investigate the distribution and concentrations of major chemicals. Afterward, a theoretical framework for the thermo-hydrodynamic process in the mine water coupled with heat transfer in the surrounding geologic formations is developed to outline a mathematical description for studying the scientific issue. Simulations are finally conducted, based on the real geologic information, to preliminarily investigate the quasi-equilibrium water movement in this local mine shaft due to geothermal gradients to provide insights into the phenomena observed in the field study.

### 1. Introduction

Geothermal energy recovery from flooded underground mines has been gaining momentum worldwide since the pioneering work in Canada in 1989 [1]. The application of the use of the water in flooded mines, i.e., mine water, as a geothermal resource is a variation of the Surface Water Heat Pump (SWHP) system [2], which falls into the category of low-temperature geothermal applications [3]. The SWHP is less common than the other Geothermal Heat Pump (GHP) systems, i.e., Ground-Water Heat Pump (GWHP) system and Ground-Coupled Heat Pump (GCHP) system, as the SWHP involves environmental and legal concerns when accessing natural waters (e.g., lake, pond, and river). Moreover, the SWHP can represent a higher-quality geothermal energy resource because bulk water provides a better medium for heat transfer than the pore water used in the GWHP and the water in pipes and backfill soils in the GCHP. As a variation of SWHP, the concept of the geothermal application in this study is to pump the water from deep abandoned mines and exchange heat between the pumped water and

buildings for heating/cooling purposes. This type of SWHP application thus takes advantage of abandoned facilities [4,5], provides more economical energy compared to the conventional heating methods (e.g., fuels) [6], and avoids many concerns with the use of natural water bodies in the conventional SWHPs [1]. But some aspects of this type of SWHP for its application need to be considered. Especially, the scientific questions behind the application are much different from those behind the conventional SWHPs, because the mine water-geologic system possibly represents a much more delicate system due to the extremely low velocity of the mobile water, high geothermal gradients, and complicated geologic and mining situations.

However, there is no doubt that the use of the mine water as a geothermal resource inherits most of the socioeconomic and environmental benefits of conventional GHP applications: safe [7], green [8], relatively renewable and adaptable [9,10]. In addition, from a technical perspective, the nature of the SWHP application with the mine water provides more attractive advantages, making it a much higher grade geothermal resource: eco-friendly and environmental utilization of

\* Corresponding author.

E-mail addresses: [tbao@mtu.edu](mailto:tbao@mtu.edu) (T. Bao), [zhenl@mtu.edu](mailto:zhenl@mtu.edu) (Z. Liu).

waste materials (abandoned mine water), higher-quality geothermal energy (higher geothermal gradient), highly efficient exploration (heat transport of bulk water), and economical utilization (utilization of existing facilities). The mine water has a unique feature which can even further magnify the above benefits: it can move due to both natural convection (caused by geothermal gradients and salinity) and forced convection (water from surrounding geologic formations, surface water, and the energy extraction process) [11,12]. This feature (i.e., bulk water movement due to both natural convection and forced convection), in fact, is very useful and highly desirable. This is because the natural convection in bulk water triggers warm water (at the bottom with a higher temperature) to move upward to heat cold water (at the top); the forced convection caused by the heat extraction process will lead to a greater temperature difference, which can further expedite this natural convection process. Therefore, the heat transfer due to this feature can exceed that in the conventional GWHPs and GCHPs by many orders. Though still far from being satisfactory, numerical simulations have been adopted to understand the underlying mechanisms. Hamm and Sabet [12] modeled the hydraulic behavior of the mine reservoir and the mine water temperature in a production shaft. Their study revealed the impact of the natural convection, the production flow rate, and the permeability of the surrounding rocks on the geothermal potential for explorations. More efforts have been made with an emphasis on several critical issues for the topic. One example is that Streb and Wieber [13] investigated the locality for extracting the mine water at a required temperature without causing a decrease in the potential of the discharge using a hydraulic model. The lifespan of the required temperature supply from the mine water in the flooded coal mines was also discussed by Arias et al. [14] and their numerical results indicated that the studied mine water-based geothermal system would serve over 30 years.

Despite several real demonstration projects launched worldwide for the mine water-based geothermal application [1,15], a thorough scientific understanding of the mechanisms associated with recovering geothermal energy from the mine water is still absent. However, such an understanding is critical to the practical implementation of the energy technique. Since economic paybacks are usually the major driving force for the application, the first two things of interest are usually what will be the water temperature available for the geothermal heat pumps (efficiency) and how will that temperature vary as the exploration proceeds (sustainability). However, as mentioned above, the mine water has a unique feature when it is considered as a geothermal resource: energy is convected by moving fluid elements of the mine water. The significance of this factor is not predictable. The major phenomenon in the mine water was summarized as ‘thermohaline staircases’ caused by a thermosolutal flow [11]. To be more specific, a buoyancy-driven flow, which results from the density difference due to temperature (thermal) and salinity (solute) differences, is proposed to be the major process of interest in the mine water. Experimental and numerical studies suggested that seepage from surrounding geological formations [1,16] and the configuration of the mine working spaces [17,18] may also play significant roles.

Due to the complexity of and limited accessibility to the underground mining space, the underlying uncertainty may only be disentangled by means of numerical simulations with the help of limited site measurements. Though not common, numerical studies have been made to investigate either the sustainability concern regarding the energy recharge from the geologic formations around the mine water [19] or the efficiency concern regarding the hydrodynamics (buoyancy-driven flow for heat variation) in the mine water [12,20]. In particular, two numerical studies have been conducted to understand non-isothermal hydrodynamics of the mine water, which is a key in this geothermal application by controlling the temperature variation and distribution. Hamm and Sabet [12] investigated the temperature variation of the mine water in a vertical shaft using non-isothermal hydrodynamics without the thermal coupling between the mine water and

the surrounding geologic formations. In the other study, Reichart et al. [11] investigated the temperature variation of the buoyancy-driven flow triggered by both temperature and salinity using a small computational scale of the mine water (around 1 m). However, the existing studies were concentrated on either geologic formations or mine water, instead of the multiphysics of the whole system. This fact is possibly attributable to several reasons: (1) the complexity of the physical mechanisms in the natural process, (2) high computational cost, and (3) limited data from the field. In addition, numerical simulation for the topic is mostly separated from field studies due to the limited accessibility to abandoned underground mines. A comprehensive study of mine water-based geothermal applications (i.e., a variation of SWHP system), including a field study, the theoretical understanding, and numerical analyses, is highly desirable. This paper will fill this knowledge gap by presenting such a study. A field test on Hancock Shaft 2 is presented in Section 2. A theoretical framework is developed in Section 3 for the thermo-hydrodynamic process in the mine water coupled with heat transfer in the surrounding geologic formations. A preliminary assessment of Shaft 2 is presented in Section 4 to shed light on the buoyancy-driven flow.

## 2. Field measurements

It is known from Section 1 that the temperature distribution within the water in deep abandoned mines is a key issue to this geothermal application. However, it is usually difficult to obtain such data. This is because abandoned underground mining working spaces may partially collapse after flooding and very limited information can be obtained regarding what structures remain after the mine is closed. Some field data are available indirectly from those environmental and mining investigations into water stratification in abandoned mines [18]. However, few field measurements can be found for the purpose of recovering geothermal energy from flooded mines, let alone field measurements conducted in parallel to other site explorations and numerical analyses.

This section introduces a field study for measuring the temperature and chemical distributions in an abandoned copper mine shaft located in the Upper Peninsula (U.P.) of Michigan. This copper mining region was the first major copper mining region in the U.S., which started in the 1840s and ceased in 1968. Hundreds of deep mines were developed during this period with some mines reaching depths of 2.4 km due to the depth of the lodes. Among them, the Quincy mine was the most famous copper mine, which had the deepest shaft worldwide (i.e., Shaft 2 in Fig. 1) with a depth of 2.82 km, when it ceased production in 1945. Another copper mine on the southwest of the Quincy mine was the Hancock mine, which had two major shafts (Shaft 1 and Shaft 2). These mines were flooded with groundwater soon after their closures and are available as potential geothermal energy resources.

Shown in Fig. 1 is the layout of the underground mining spaces of the Quincy mine and the Hancock mine close to the downtown of the Hancock City in the state of Michigan in the U.S. The 3D underground mining structures are projected to the map for visualization. The black lines from the southeast (top) to the northwest (bottom) are the major mine shafts, e.g., Hancock Shaft 2 and Quincy Shaft 7 (projection). The red lines are the horizontal drifts (projection) from the southwest to the northeast. The drifts are approximately parallel to each other and perpendicular to the shafts. The shafts are connected by the horizontal drifts. In this study, a nearly vertical shaft, i.e., Hancock Shaft 2 in the lower left corner of Fig. 1, was chosen for the field test. The field measurement location was marked with a red dot, which is located in the Hancock City.

Technically, the Hancock Shaft 2 was not “abandoned” but sealed many decades ago. The excavation for the shaft was started in December of 1906, which reached 400 feet (122 m) deep by the end of the year. By November of 1908, it reached 1300 feet (396 m) with the shaft being sunk to the massive dimensions of 29' 6" by 9' 6" (9 m by

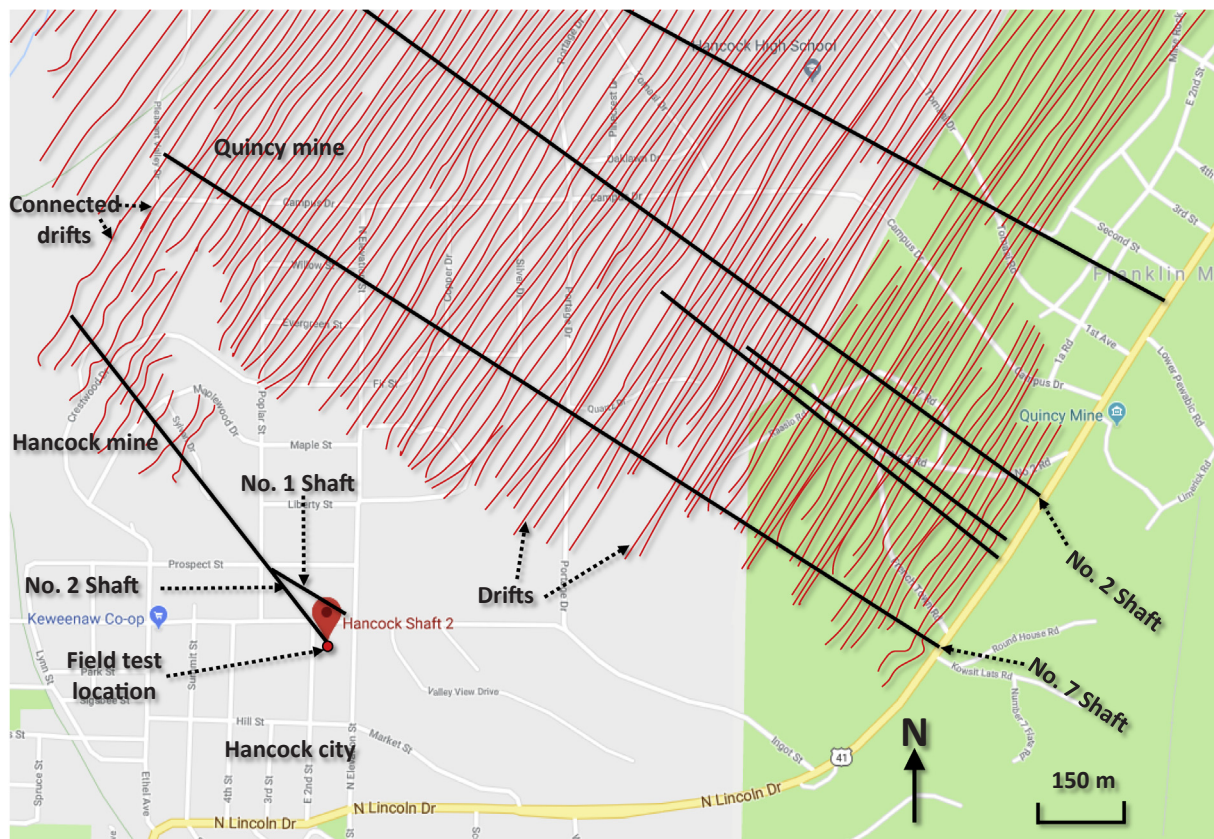


Fig. 1. Layout of underground mining spaces of Quincy and Hancock mines [Developed with Google map].

2.9 m) and contained four hoisting compartments and one service duct. Another main shaft in the Hancock mine group, i.e., Hancock Shaft 1, is close to Hancock Shaft 2. These two shafts are connected on the 13th level. In 1915, the 63rd level of the Hancock Shaft 2 at a depth of 1 km was drilled through to a drift that corresponds the drift of the Quincy Shaft 7 to form the connected drift (see Fig. 1), and the two were, from then on, worked as one. The final depth of the Hancock Shaft 2 was estimated to be 4000 feet (1219.2 m).

There is a practical reason for choosing this vertical shaft, though it is not typical in the U.P.: it is very hard to lower equipment down into the shaft which could be over thousands of meters long. Attempts have been made in the U.P. to send robots down non-vertical shafts, which might overcome this issue. However, it was found that most parts of the submerged mining structure are covered with a thin layer of silt and the propulsion of the robot can easily stir the silt up and make the mine water almost invisible. Therefore, this vertical shaft was chosen for the test.

Sensors for temperature and electrical conductivity were sent down into the shaft using a pulley system, which is similar to the wireline system in the oil industry [21,22]. Based on one ongoing real project for this geothermal application in the U.P., it was estimated that 1000 feet (305 m) are a limit, beyond which pumping costs would overcome the economic gain of the geothermal application with the mine water in the U.P. Notwithstanding, the sensors were lowered to a depth slightly over 3000 feet (914 m) for a better understanding of the water movement and temperature distribution. The temperature transducers had a slow response time to a temperature change. The depth was not recorded with the temperature transducer. But instead, the best effort was made to correlate the temperature and the depth based on time. An encoder was deployed on the pulley system to accurately calibrate for depth. Two temperature sensors, i.e., the HOBO U12 stainless temperature data logger and the Aqua TROLL 200 temperature sensor, were used. The HOBO temperature sensor has a measurement range of  $-40^{\circ}\text{C}$  to

$125^{\circ}\text{C}$  and can work appropriately under a maximum pressure of 2200 psi. Its measurement resolution is  $0.03^{\circ}\text{C}$  in the measurement range of  $0\text{--}20^{\circ}\text{C}$  and its accuracy is  $\pm 0.25^{\circ}\text{C}$  in the measurement range of  $0\text{--}50^{\circ}\text{C}$ . The Aqua temperature sensor has a measurement resolution of  $0.01^{\circ}\text{C}$  and an accuracy of  $\pm 0.1^{\circ}\text{C}$ . It has a maximum working pressure of 500 psi and a measurement range of  $-5^{\circ}\text{C}$  to  $50^{\circ}\text{C}$ . The Aqua TROLL 200 conductivity sensor was utilized for electrical conductivity measurements. This sensor has a measurement range of  $5\text{--}100,000\ \mu\text{S}/\text{cm}$ . Its measurement accuracy and resolution are  $\pm 1.005\ \mu\text{S}/\text{cm}$  and  $0.1\ \mu\text{S}/\text{cm}$ , respectively. The above three sensors were all internal memory data logging devices and were calibrated before the test. A pressure gauge (related to depth) was used to ensure that the sensors were not “hung up” on anything.

The measured variations of the temperature and electrical conductivity with depth are shown in Fig. 2. It is seen that the water level is at 200 feet (60 m) below the ground surface. Therefore, data at positions above that point are of limited value. The water temperature is not linearly distributed along the depth, as predicted for stagnant water surrounded by rocks with a linear temperature distribution because of an approximately constant geothermal gradient. Instead, the data clearly demonstrate the existence of two constant temperature zones with an average temperature of  $54.7^{\circ}\text{F}$  ( $12.6^{\circ}\text{C}$ ) and  $59.3^{\circ}\text{F}$  ( $15.2^{\circ}\text{C}$ ), respectively. The existence of the two constant temperature zones indicates that the water is stratified. This stratification is also supported by the distribution of the electrical conductivity. The value of the electrical conductivity indirectly reflects the distribution of the total salt concentration. As can be seen, the changes in the temperature and electrical conductivity happen at about the same depths. The distributions of both the temperature and electrical conductivity led us to the same deduction: water moves relatively fast within individual layers (zones or cells) and consequently, resulting in a constant temperature and electrical conductivity in each layer. There are slight differences in the temperatures measured by different sensors and in those measured

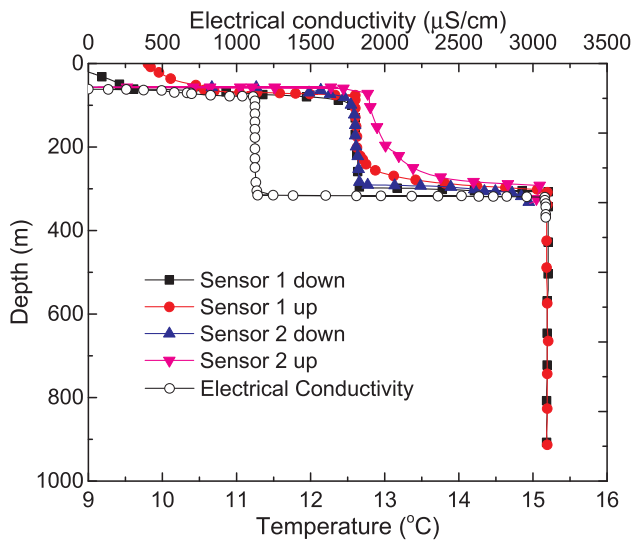


Fig. 2. Measured distributions of temperature and electrical conductivity.

by the same sensor but in different runs (i.e., up or down). The major reason is the slow temperature response of the transducers that were continuously raised or lowered, leading to temperature-depth profiles that are not highly accurate.

In order to provide cross-references, water was sampled at 200 (61 m), 577 (176 m), 750 (229 m), 1000 (305 m), and 3000 (914 m) feet using a Kemmerer water sampler. The numbers of collected samples from the above corresponding depths were one, three, four, five, and six, respectively. The samples were analyzed at the White Water Associates in Amasa (certification number #65802), Michigan. pH and alkalinity were measured with potentiometry using a standard hydrogen electrode (standard method 4500-H + B) and with the Titration Method (standard method 2320B), respectively. The metals contained in the samples were determined with the standard method 6010B using an Inductively Coupled Plasma (ICP). The Method Detection Limit (MDL), which determines the minimum concentration of a substance with 99% confidence, was used to evaluate the measurement accuracy. All the measurements were conducted by the White Water Associates under the procedure of each standard method. The results from the measurements present direct evidence for the distributions of different minerals in the mine water. As shown in Table 1, the results support the deduction obtained above regarding the water stratification. More than that, the results from Table 1 also help provide a direct estimate of the quality of the mine water in the site for the safe use, which is another concern for exploring the mine water for geothermal applications. The concern could be raised when the acid mine water is pumped out and chemicals, such as heavy metals, are stirred up or pumped out from the mine water in the deep mining space. Table 1 shows that the concentration of Mn varies with depth, where it is less than 0.53 mg/L

before 1000 feet (305 m) and increases to 1.6 mg/L at the depth of 3000 feet (914 m). The above values of the concentration of Mn are much lower than the upper limit value (59 mg/L) calculated using Rule 57 for evaluating the quality of non-drinking surface water according to Department of Environmental Quality, Michigan. In addition, according to Piatak et al. [23], the range of pH values for water samples collected from the Pike Hill copper mines in Vermont in the U.S. is 3.1–4.2, which is undesirable as it is too acid. However, as shown in Table 1, the range of the measured pH of this mine water is 6.8–7.1. Such a range is very safe as the mine water is close to neutral rather than acid. This is because the mine water quality possibly has rebounded due to the mine water “rebound” process (i.e., flooding) with low alkaline (pH range:7.0–7.5 according to [24]) water in the local area. Therefore, the range of the measured pH of this mine water is very close to the local surface water.

### 3. Theoretical formulation of the underlying mechanisms

From a multiphysics viewpoint, the scientific understanding of the problem in this study possibly involves heat transfer, water movement, particle transport, chemical reactions, and mechanical responses in both the mine water and the surrounding geologic formations. It is a so-called thermo-hydro-diffuso-chemico-mechanical problem in the water-geologic formation system [11,16]. However, a comprehensive consideration of the above mechanisms is nearly impossible due to constraints in the computational resources. It is believed that hydrodynamics in the mine water is a critical part of the geothermal energy recovery while the multiphysical processes in the geologic formations are possibly much less significant in this application. In addition, multiphysics frameworks in porous materials have been successfully implemented and validated in the previous studies, e.g., Liu and Yu [25] and Liu et al. [26], therefore, it is less urgent to implement such multiphysics frameworks in this study. Due to the above considerations, the focus in this paper is placed on the hydrodynamics of the mine water.

A few numerical studies have been conducted previously to evaluate the efficiency of the energy application by studying the hydrodynamics (buoyancy-driven flow) in the mine water or to investigate the sustainability of the system by studying the heat transfer in the geologic formations [12,20]. However, these studies for heat transfer are focused on either the mine water or the geologic formations and consequently, they fail to reflect the real thermal field in the system. In fact, the whole mine water-geologic formation system needs to be considered by including the hydrodynamics in the mine water, heat transfer in the surrounding geologic formations, and their couplings.

To capture these mechanisms, this section outlines a theoretical framework for the thermo-hydrodynamic process in the mine water coupled with heat transfer in the surrounding geologic formations. Overall, this framework is intended for a multiphysical process involving the thermal field in both the geologic formations and the dynamics of water movement in an open mining space. The thermo-

Table 1  
Measured results for chemical concentrations in the mine water.

| Depth | CO <sub>3</sub><br>mg/L | HCO <sub>3</sub><br>mg/L  | pH  | mg/L     | Cl       | F        | Fe      | Mn           | Na        | K            | NO <sub>2</sub> NO <sub>3</sub> | SiO <sub>2</sub> | SO <sub>4</sub> |
|-------|-------------------------|---------------------------|-----|----------|----------|----------|---------|--------------|-----------|--------------|---------------------------------|------------------|-----------------|
| Feet  | Carbonate<br>Alkalinity | Bicarbonate<br>Alkalinity | pH  | Hardness | Chloride | Fluoride | Iron(t) | Manganese(t) | Sodium(t) | Potassium(t) | Nitrate<br>Nitrite-<br>N        | Silica(d)        | Sulfate         |
| 200   | 0                       | 190                       | 7.1 | 300      | 170      | 0        | 1       | 0.12         | 41        | 0.97         | 0.22                            | 15               | 37              |
| 577   | 0                       | 200                       | 6.9 | 470      | 280      | 0        | 14      | 0.52         | 62        | 0.85         | 0                               | 16               | 0               |
| 750   | 0                       | 200                       | 7.1 | 450      | 280      | 0        | 11      | 0.46         | 61        | 0.78         | 0                               | 17               | 0               |
| 1000  | 0                       | 200                       | 7.1 | 490      | 310      | 0        | 11      | 0.53         | 64        | 0.77         | 0                               | 17               | 0               |
| 3000  | 0                       | 210                       | 6.8 | 1300     | 920      | 0        | 34      | 1.60         | 150       | 0.87         | 0                               | 33               | 0               |
| MDL   | 5                       | 5                         | 0.1 | 0.3      | 4        | 0.006    | 0.01    | 0.0013       | 0.15      | 0.12         | 0.1                             | 0.03             | 15              |

Note: MDL = Method Detection Limit.

hydrodynamic framework includes the transient natural convective motion of water and heat in the system. The transport of salts is also included in this theoretical framework but is not considered in the later simulations. The governing mechanisms in the system can be mathematically described by a multiphysics framework as follows.

The movement of the mine water in deep underground mining spaces could be considered as large-scale hydrodynamics. For this large-scale hydrodynamics, water can be reasonably assumed to be incompressible. The continuity equation for the incompressible flow is formulated as

$$\nabla \cdot \mathbf{U} = 0 \quad (1)$$

where  $\mathbf{U}$  is the velocity of the mine water (m/s). The momentum balance of water is described as

$$\frac{\partial \mathbf{U}}{\partial t} + \nabla \cdot (\mathbf{U}\mathbf{U}) - \nabla \cdot \left[ \frac{\mu_{eff}}{\rho} (\nabla \mathbf{U} + \nabla \mathbf{U}^T) - \frac{2}{3\rho} \mu_{eff} (\nabla \cdot \mathbf{U}) \mathbf{I} \right] = -\frac{1}{\rho} (\nabla p_d - \rho_{eff} \mathbf{g}) \quad (2)$$

where  $\rho$  is the density of the mine water (kg/m<sup>3</sup>);  $\mathbf{I}$  is the identity matrix;  $\mu_{eff}$  (Pa s) is the effective viscosity represented using  $\mu_{eff} = \mu_{laminar} + \mu_{turbulent}$ , in which  $\mu_{laminar}$  and  $\mu_{turbulent}$  are the laminar dynamic viscosity and the turbulent dynamic viscosity, respectively;  $p_d$  is the dynamic pressure (Pa) and is formulated by  $p_d = p - \rho g h_e$ , in which  $g$  is the acceleration (m/s<sup>2</sup>),  $h_e$  is the elevation (m), and  $p$  is the total pressure (Pa); and  $\rho_{eff}$  is the effective density (kg/m<sup>3</sup>), which is a function of temperature  $T$  (K) and salinity  $S$  and can be described using the following equation

$$\rho_{eff} = \rho_{eff}(T, S) \quad (3)$$

The governing equation for salt transport is formulated as

$$\frac{\partial S}{\partial t} + \mathbf{U} \cdot \nabla S = \nabla \cdot (\alpha_s \nabla S) \quad (4)$$

where  $\alpha_s$  is the solute diffusivity coefficient of the mine water (m<sup>2</sup>/s), which is given by  $\alpha_s = \alpha_{laminar}^S + \alpha_{turbulent}^S$ . Generally, the salinity of the mine water increases with depth, leading to a higher density in the salty water when compared to the fresh water. The fresh water thus overlays the salty water. This suppresses the natural convection in the mine water. The governing equation for salt transport is presented here to complete the framework. For simplicity, the difference in the mine water due to salinity is excluded in the later simulations in this study.

The energy conservation within the moving fluid element can be formulated in terms of the temperature  $T$  (K) as follows

$$\frac{\partial T}{\partial t} + \mathbf{U} \cdot \nabla T = \nabla \cdot (\alpha_T \nabla T) \quad (5)$$

where  $\alpha_T$  is the thermal diffusivity of the mine water (m<sup>2</sup>/s) and is given by  $\alpha_T = \alpha_{laminar}^T + \alpha_{turbulent}^T$ .

Heat transfer in the surrounding geologic formations is coupled to the heat transfer in the mine water. To be more specific, the heat conduction happens across the interface between the surrounding geologic formations and the mine water if the temperatures on two sides of the interface are different. Thermal conduction in geologic formations is governed by the following equation

$$\rho_s c_p \frac{\partial T}{\partial t} = \nabla \cdot (k_s \nabla T) \quad (6)$$

where  $\rho_s$  is the solid density (kg/m<sup>3</sup>),  $c_p$  is the specific heat of the solid (J/(kg K)),  $k_s$  is the thermal conductivity of the solid (W/(m K)). Fig. 3 illustrates the thermal coupling process at the interface between the two regions, i.e., the mine water and its surrounding geologic formations. As can be seen, the energy rate  $\phi_w$  via convection for the mine water and the energy rate  $\phi_c$  via conduction for the surrounding rocks are formulated as

$$\phi_w = hA(T_i - T_{wc}) \quad (7)$$

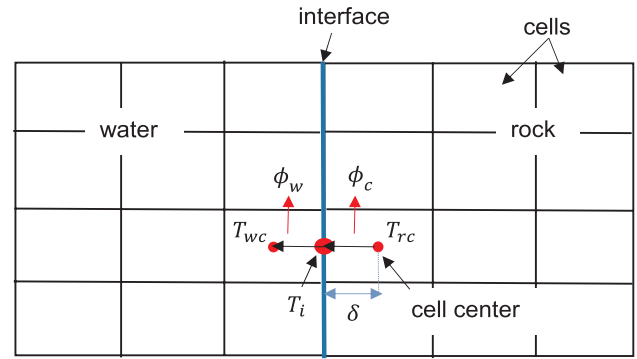


Fig. 3. Schematic of thermal coupling between the mine water and surrounding rocks.

$$\phi_c = \frac{k_s}{\delta} A (T_{rc} - T_i) \quad (8)$$

where  $h$  is the convective heat transfer coefficient (W/(m<sup>2</sup> K)),  $A$  is the area (m<sup>2</sup>),  $T_i$  is the temperature at the interface,  $T_{wc}$  and  $T_{rc}$  are the cell-center temperature in the water region and the solid region adjacent to the interface, respectively, and  $\delta$  is the distance (m) between the face-center (the center of a face of a finite volume cell) at the interface and the cell-center in the solid region. At the interface,  $\phi_w = \phi_c$ , we obtain

$$T_i = \frac{k_s \delta}{h + k_s \delta} T_{rc} + \frac{h}{h + k_s \delta} T_{wc} \quad (9)$$

At every iteration, Eq. (9) was used to determine the temperature at the interface, which will be used as the boundary temperature to solve a transient heat equation in each region. The value of  $k_s$  is a constant and estimated according to [27] (see Table 2 in Section 4) while the initial values of  $h$  for each cell are calculated with Eq. (7) using the given initial  $T_i$  at the first iteration. After that, the values of  $h$  (calculated using  $T_i$  from the last step) and  $T_i$  are updated automatically via iterations. In such a way, the interface between the two regions is thermally coupled.

#### 4. Preliminary assessment of the Hancock shaft 2

The above section laid down a theoretical framework for simulating the complicated physical processes in the mine water-surrounding geologic formation system. The following work was carried out to meet the urgent need for testing the performance of the above framework for hydrodynamics in a mine water environment affected by the heat from the surrounding rocks, especially for the buoyancy-driven flow, which is believed the dominant mechanism. The purpose is to reproduce the quasi-equilibrium water movement process, in which the mine water is well mixed due to the temperature difference caused by the geothermal gradient. Moreover, it will be of practical interest if simulations based on the theoretical framework can provide insights into the data obtained from the field study introduced in Section 2, even though a direct comparison is difficult due to the lack of data. Such transient simulations have been conducted and preliminary results are presented in this section.

Thermo-hydrodynamic modeling of the mine water in the Hancock Shaft 2 in the U.P. was preliminarily implemented. According to Butler and Burbank [28], as shown in Fig. 4, the Hancock Shaft 2 is nearly vertical and connects eight horizontal drifts at different depths. Shaft 1 is also connected with Shaft 2 via the upper drifts, where faults are located. It is known that the geometry of these horizontal drifts is extremely irregular due to those faults and blasting activities, so is that of the shafts. A cylindrical shaft and drifts were adopted in the current simulation for analyses in this study, which is similar to the previous studies, e.g., Hamm and Sabet [12], without considering Shaft 1 and those faults, as shown in Fig. 5. As can be seen, the configuration and

**Table 2**  
Parameters used in the current simulation.

| Conglomerate type |        | Thermal conductivity (W/(m K)) | Specific heat (J/(kg K)) | Density (kg/m <sup>3</sup> ) | Reference density (kg/m <sup>3</sup> ) | Reference temperature (K) | Specific heat (J/(kg K)) | Prandtl number | Dynamic viscosity (Pa s) |                         |
|-------------------|--------|--------------------------------|--------------------------|------------------------------|--|---------------------------|--------------------------|----------------|--------------------------|-------------------------|
| Rock              | No. 16 | 1.69                           | 841                      | 2800                         | Mine water                             | 999.8396                  | 273.15                   | 4181           | 6.62                     | 9.59 × 10 <sup>-4</sup> |
|                   | No. 17 | 1.58                           | 839                      |                              |  |                           |                          |                |                          |                         |
|                   | No. 18 | 1.57                           | 843                      |                              |  |                           |                          |                |                          |                         |
|                   | No. 22 | 1.22                           | 840                      |                              |  |                           |                          |                |                          |                         |

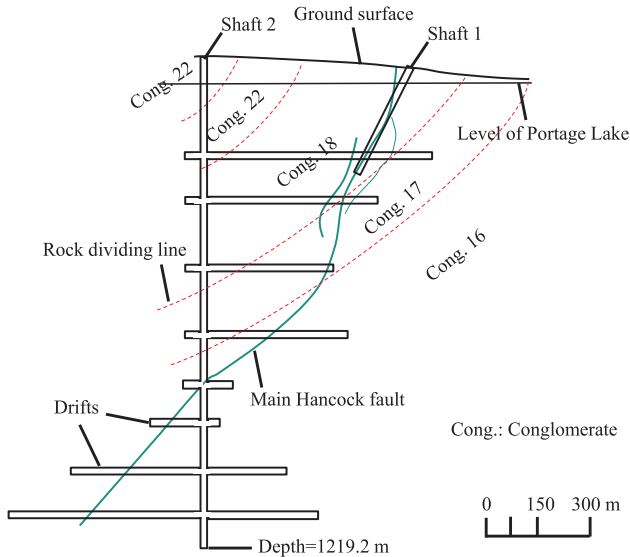


**Fig. 4.** Cross-sectional view of the layout of the Hancock mine according to [28].

position of the shaft and drift were determined based on the real geologic conditions in Fig. 4. The dimensions of the shaft were adopted according to the documented data [28], while the dimensions of drifts were assumed based on Hamm and Sabet [12]. To allow for the complicated geologic conditions, the surrounding rocks include major rock layers, i.e., conglomerate No. 22, No. 18, No. 17 and No. 16, according to Fig. 4. The water level is 60 m below the ground surface according to

the field data in Fig. 2, soils and the rocks above the water surface in the mine, therefore, were not included in this case. The geologic formations were only rocks in the simulation. The total length of the mine water in the shaft is 1159.2 m, as shown in Fig. 5. In addition to the surrounding rocks, the bottom rocks (conglomerate No. 16) that are in contact with the bottom surface of the mine water were included. The coupling between the mine water and the surrounding rocks deserves special attention. This is because heat transfer occurs cross those two regions and affects the movement of the mine water via conduction. This coupled heat transfer between two regions was solved using Eq. (9) introduced in Section 3. For the dimension of finite volume cells, the model was configured with a high resolution of 1.5 m (i.e., side length of the cell) for the mine water body and the rock regions in the proximity of the mine water, while the rocks far from the mine water were discretized with a relatively low resolution of 3–5 m.

To consider the geothermal gradient at the domain, the internal temperature in both the water body and the surrounding rocks was assumed to be linearly distributed with depth from 282.15 K (9 °C) to 288.15 K (15 °C), in which the temperature was adopted according to the field study in Fig. 2. The temperature of the bottom rocks (200 m × 754 m × 50 m (x × y × z)) was assumed to be uniform within the domain and fixed at 288.15 K at the bottom. Our trial calculations indicated that the temperature variations in the surrounding rocks (200 m × 754 m × 1159.2 m) only occur within a few tens of meters away from the shaft. Due to this reason, a Neumann type of boundary with no heat flux was used at the exterior side boundaries of the surrounding rocks. For the hydrodynamics, the dependence of the water density on temperature is a critical auxiliary relationship, which determines the overall process of the buoyancy-driven flow. As introduced above, salinity will not be included in this case. The classic

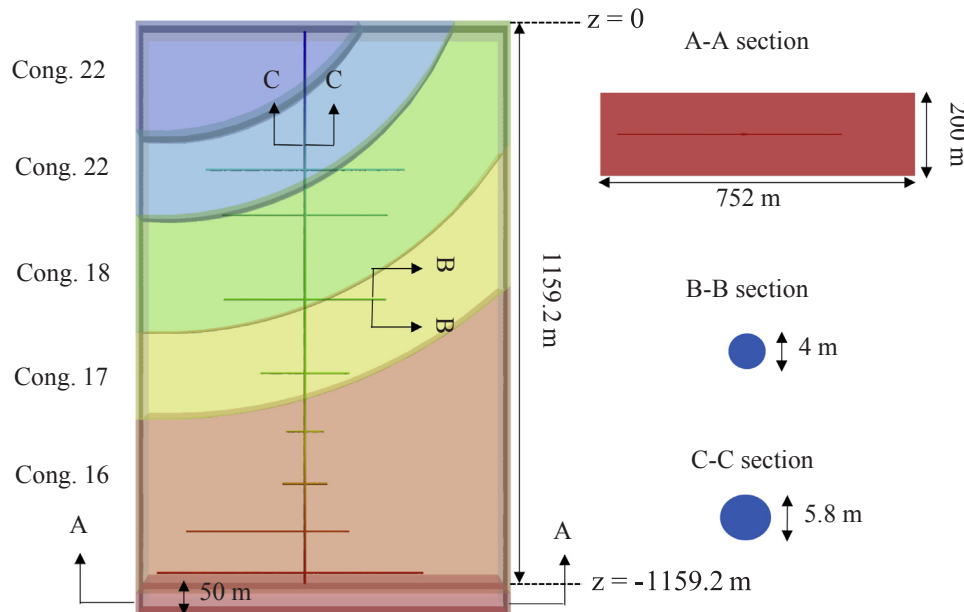


**Fig. 5.** Configuration of the mine water-layered rocks system and its dimensions (the red line in A-A section is the projection of the bottom drift on the bottom rocks).

Boussinesq approximation was used to formulate the relationship between the fluid density and temperature, in which this relationship is assumed to be linear. The effective density  $\rho_{eff}$  is formulated using a reference density at a reference temperature and the thermal expansion coefficient  $\beta$  ( $K^{-1}$ ) in the following equation [29]

$$\rho_{eff} = \rho_{ref} [1 - \beta (T - T_{ref})] \tag{10}$$

where  $\rho_{ref}$  is the reference density and  $T_{ref}$  is the reference temperature. The simulation was conducted by implementing the framework outlined in Section 3 with an open-source finite volume method C++ library, OpenFOAM. The PISO algorithm was used in this study to solve the iteration of the system [29,30]. The framework validation is not presented here but can be found in detail in the study of [31]. The laminar flow was considered in the current simulation. The thermodynamic properties of the mine water slightly vary with the temperature. However, this temperature dependence of the thermodynamic properties of the mine water was treated as negligible in this study except for  $\rho_{eff}$  in Eq. (2). The thermal conductivity of the rocks varies with the porosity [32]. According to Manger [33], the porosity of sedimentary conglomerates has a range of 0.5–1.1%. The existence of water in voids of the rocks also influences the thermal conductivity of the rocks [27]. The thermal conductivities of the sedimentary rocks in this study were estimated within the above porosity range considering water in voids of the rocks according to Robertson [27]. The parameters used in this case are detailed in Table 2. Due to the high computational cost of the large-scale simulation, this study investigates a process lasting 46 days.

Simulation results for the initial and final temperature contours of the system are depicted in Fig. 6. As can be seen in Fig. 6a, the initial internal temperature distributions in the mine water and the surrounding rocks are identical and linear with depth because they were defined to have the same linearly distributed internal temperature from 282.15 K (9 °C) to 288.15 K (15 °C). After 46 days, the temperature

distribution in the mine water changes obviously because of the natural thermal convection caused by the density difference in the mine water (Fig. 6b). The temperature distribution in the surrounding rocks, however, almost remains unchanged. This comparison indicates that the natural convection, which only exists in the mine water, is a much more dominating heat transfer mechanism in the mine water. Without it, the rate of heat transfer in the mine water would be comparable to that in the rocks.

Typical simulation results for the flow patterns at different times in two representative areas, i.e., Region A and Region B in Fig. 6b, are depicted in Figs. 7 and 8, respectively. Due to the density difference caused by the geothermal gradient, the mine water is not stagnant. As can be seen in Figs. 7 and 8, the mine water circulates in the shaft. To be more specific, the water at the bottom with high temperatures moves upwards, because this water is relatively lighter compared to that at the top with low temperatures. By contrast, the water at the top with low temperatures moves down. Then the water from the bottom is mixed with and cooled by the cold water at the top. The water from the top is mixed with and heated by the warm water at the bottom. The water, which has been cooled at the top, tends to be heavier and therefore moves down and returns to the bottom. This water circulation is faster at  $t = 1$  h and 1 day when compared to those at  $t = 15$  and 46 days, which can be seen from the magnitudes of the velocity of the mine water. This larger velocity is caused and triggered by the larger temperature difference defined in the initial condition. As time elapses, the temperature difference decreases. Overall, this water circulation is triggered by the geothermal gradient and will approximate a quasi-equilibrium state gradually in which water is moving by following a relatively stable pattern.

On the other hand, the surrounding rocks influence the mobile mine water via heat conduction. Fig. 9a presents temperature distributions along the horizontal axis in Fig. 6 through both the surrounding rocks and the mine water at an evaluation of 5 m below the mine water

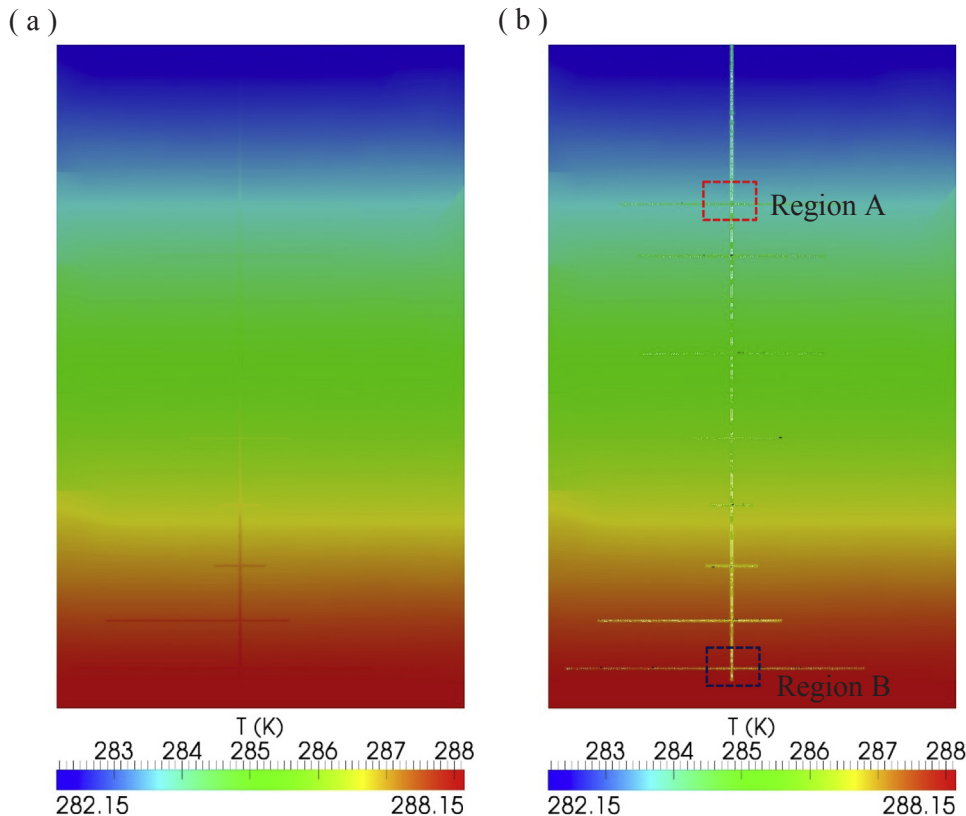


Fig. 6. Temperature profiles of the system: (a) initial conditions and (b)  $t = 46$  days.

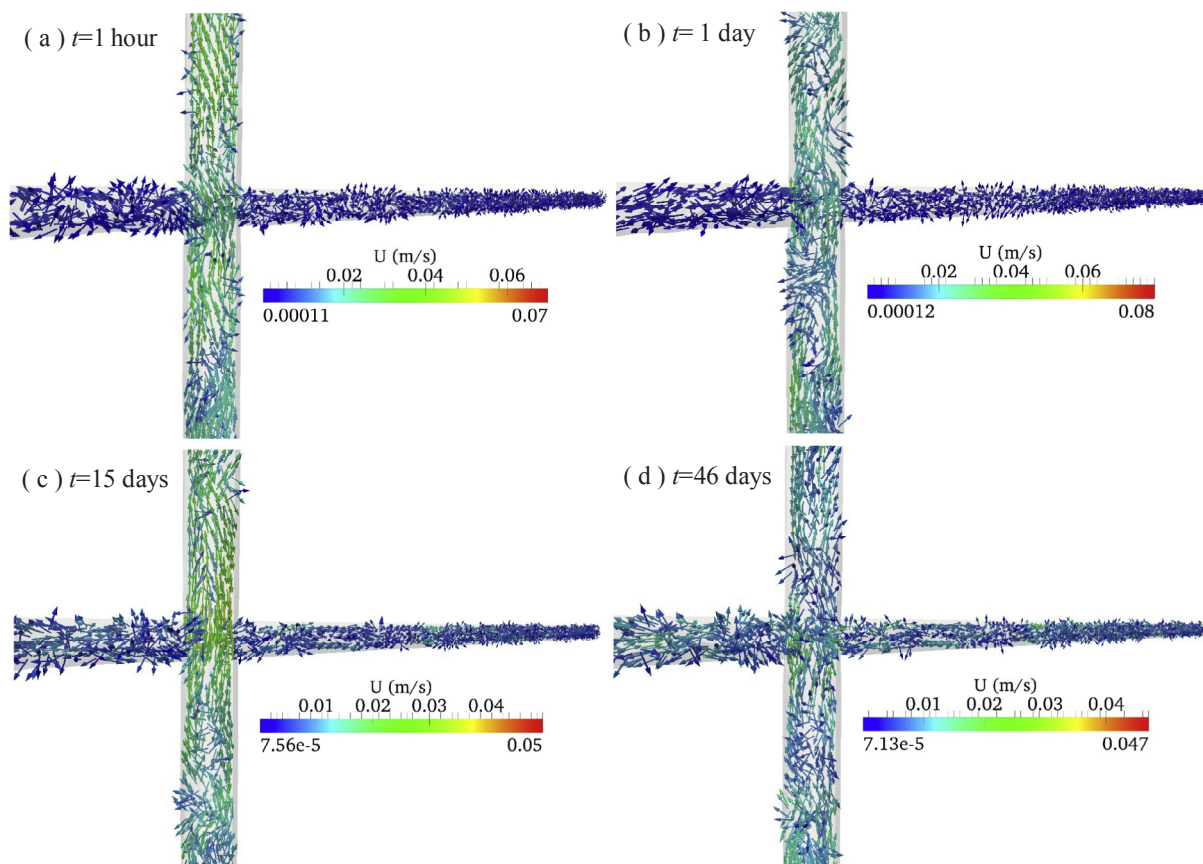


Fig. 7. Flow patterns of Region A in the water body: (a)  $t = 1$  h, (b)  $t = 1$  day, (c)  $t = 15$  days and (d)  $t = 46$  days. Note that for visualization, the temperature profile of the water body is not included.

surface ( $z = -5$  m). As can be seen, the temperature along this horizontal axis is same at  $t = 0$ , except for regions at two sides due to the effect of boundary conditions. Because of the circulation of the mine water caused by the temperature difference, the temperature of the mine water increases significantly from 282.17 K to 284.3 K within 46 days. During this period, the surrounding rocks at  $z = -5$  m affect the mine water via heat conduction. However, this conduction to the mine water is much less significant when compared to heat convection in the mine water, because the temperature of the rocks at the interface also increases (Fig. 9a). This can also be seen in Fig. 9b via the temperature variation of the node at the interface between the mine water and the surrounding rocks. The surrounding rocks at  $z = -5$  m are intended to make the mine water stable at this elevation via heat conduction to this node. However, Fig. 9b shows that the temperature of the node increases quickly rather than remains stable. This observation further indicates that heat conduction from the surrounding rocks to the mine water is not predominant when compared to heat convection. This heat convection in the mine water, therefore, dominates the thermal process of the mine water.

The temperature distributions on different cross-sections at different times can help understand how the thermal energy of the mine water is distributed and varies in a three-dimensional way, which triggers and maintains the buoyancy-driven flow. The temperature contours of the mine water on the horizontal cross-sections at the top, middle and bottom of the shaft are plotted in Figs. 10–12, respectively. As can be seen in Fig. 10a, at  $t = 0$ , the temperature is the same in the cross-section at the top. To solve the coupled heat transfer at the interface between the mine water and the surrounding rocks, the initial temperature value of 282.15 K is defined at this interface, while the temperature in the water body along the shaft is linearly distributed with depth from 282.15 K (9 °C) (top) to 288.15 K (15 °C) (bottom). Due to

this reason, at  $t = 0$ , the temperature is not the same in the cross-sections in the middle (Fig. 11a) and at the bottom (Fig. 12a). This also leads to the temperature difference on these three cross-sections (top, middle, and bottom) at  $t = 0$ . As time elapses, the temperature at the top increases from 282.15 K to 282.33 K at  $t = 3$  h. The temperature in the top cross-section continuously increases to 284.31 K at  $t = 46$  days, as shown in Fig. 10. The opposite phenomenon was observed in the cross-section at the bottom in Fig. 12. The temperature at the bottom decreases from 288.15 K to around 287 K when  $t = 46$  days. The temperature in the middle cross-section almost remains unchanged during the same process, as shown in Fig. 11. This is because the water movement will approach a quasi-equilibrium state gradually to form one layer with almost the same temperature. Eventually, this temperature is approximately equal to the initial temperature in the cross-section in the middle. It is also seen that the temperature contours, e.g., Figs. 10b or 12b, are not symmetric. This is because the relatively large (resolution is around 1.5 m) and unstructured (tetrahedron) cells were used in the simulations for the mine water to save the computational cost. Therefore, the asymmetric temperature contours were observed in Figs. 10 and 12.

At  $t = 3$  h,  $t = 1$  day or  $t = 46$  days, the temperatures in the cross-section at the top and bottom are non-uniform, as shown in Figs. 10 and 12. The reason is that the surrounding rocks with a relatively low temperature cool the mine water at the top, while the surrounding rocks with a relatively high temperature heat the mine water at the bottom. These rocks affect the temperature of the mine water via heat conduction. However, this heat conduction is much slower than the heat convection in the mine water. As a result, the temperature of the mine water varies significantly. At  $t = 46$  days, the difference between the temperatures at the top and bottom is approximately 2.5 K. These temperature variations at the top and the bottom further confirmed that

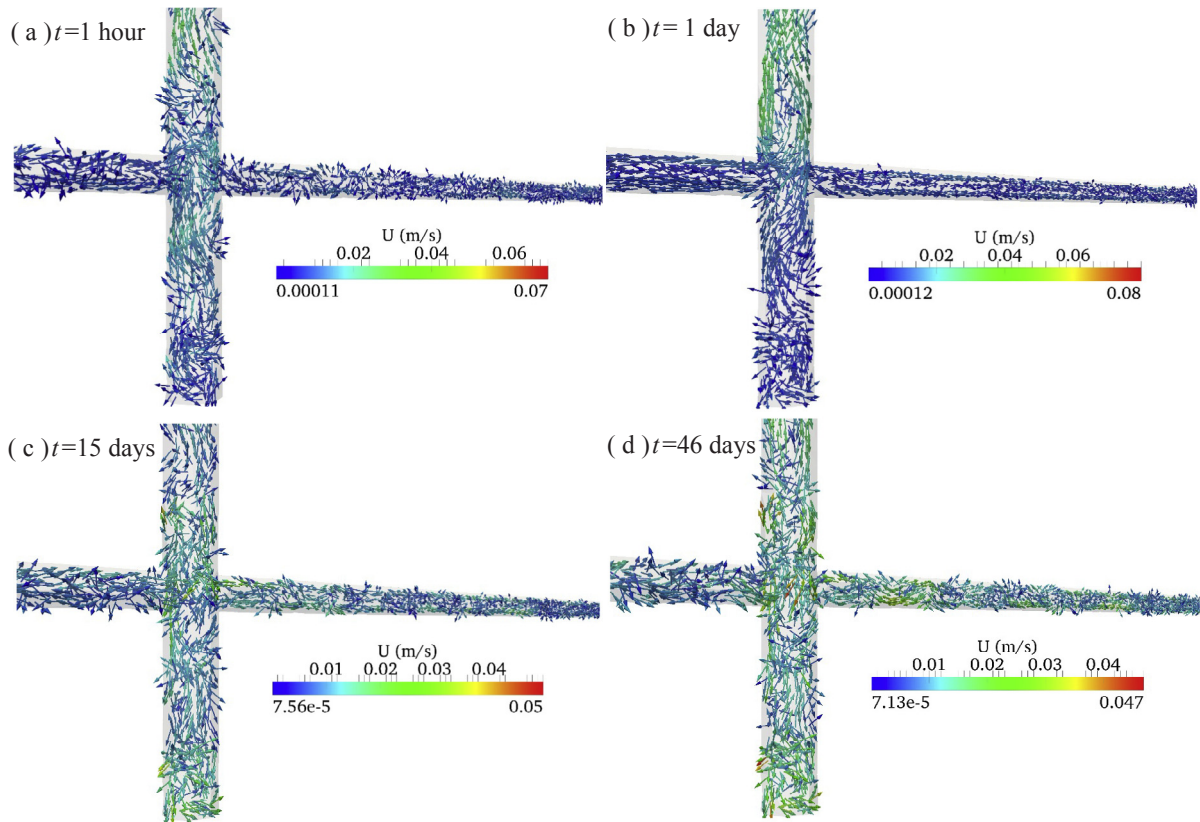


Fig. 8. Flow patterns of Region B in the water body: (a)  $t = 1$  h, (b)  $t = 1$  day, (c)  $t = 15$  days and (d)  $t = 46$  days. Note that for visualization, the temperature profile of the water body is not included.

the warm water and the cold water in the shaft are well mixed to a nearly uniform temperature. As a result, the quasi-equilibrium water movement status will be approached and maintained.

Another angle for directly showing the energy and mass flow within the mine shaft is the temperature variations with time. Five representative positions were chosen from the axis of the shaft water body to investigate the temperature variations with time. As shown in Fig. 13a, the temperature at  $z = -1159.2$  m ( $z = 0$  m on the surface of

the mine water and  $z = -1159.2$  m at the bottom of the mine water) decreases rapidly at the beginning and relatively slowly afterward. The opposite temperature variation was obtained for the temperature at  $z = 0$  m, which increases rapidly at the beginning and then slowly. The results at  $z = -289.8$  m and  $z = -869.4$  m exhibit a similar trend to those at  $z = 0$  m and  $z = -1159.2$  m. However, the temperature at  $z = -579.6$  m almost remains unchanged. These results help explain the simulated flow pattern in Figs. 7 and 8. The temperature

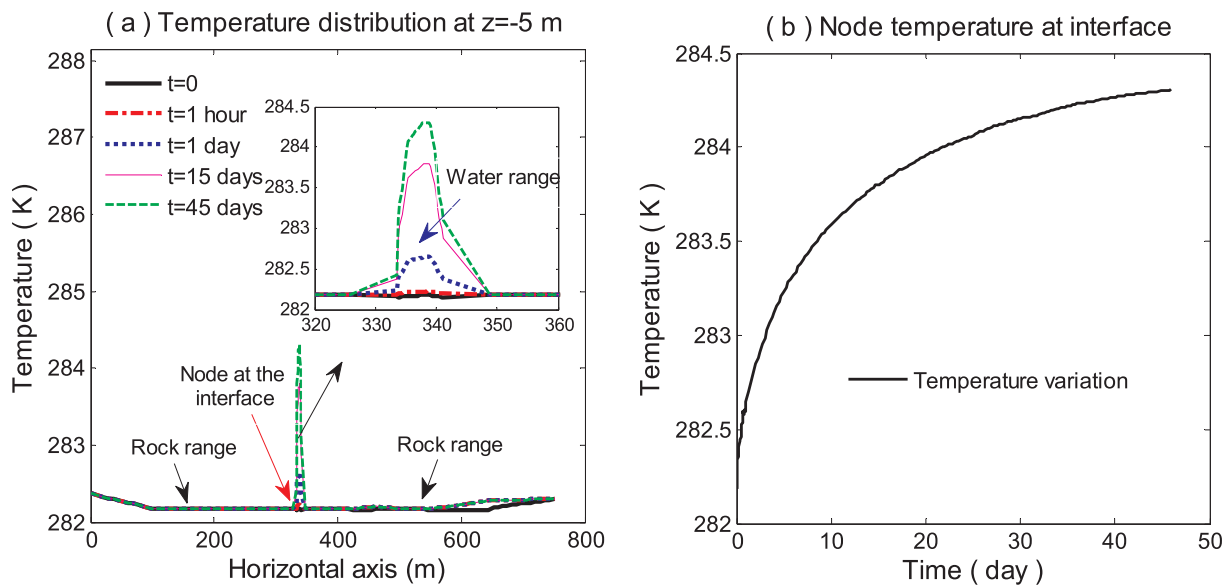


Fig. 9. Temperature changes in the domain: (a) temperature distributions along the horizontal axis through the domain at  $z = -5$  m and (b) temperature variation of the node at the interface.

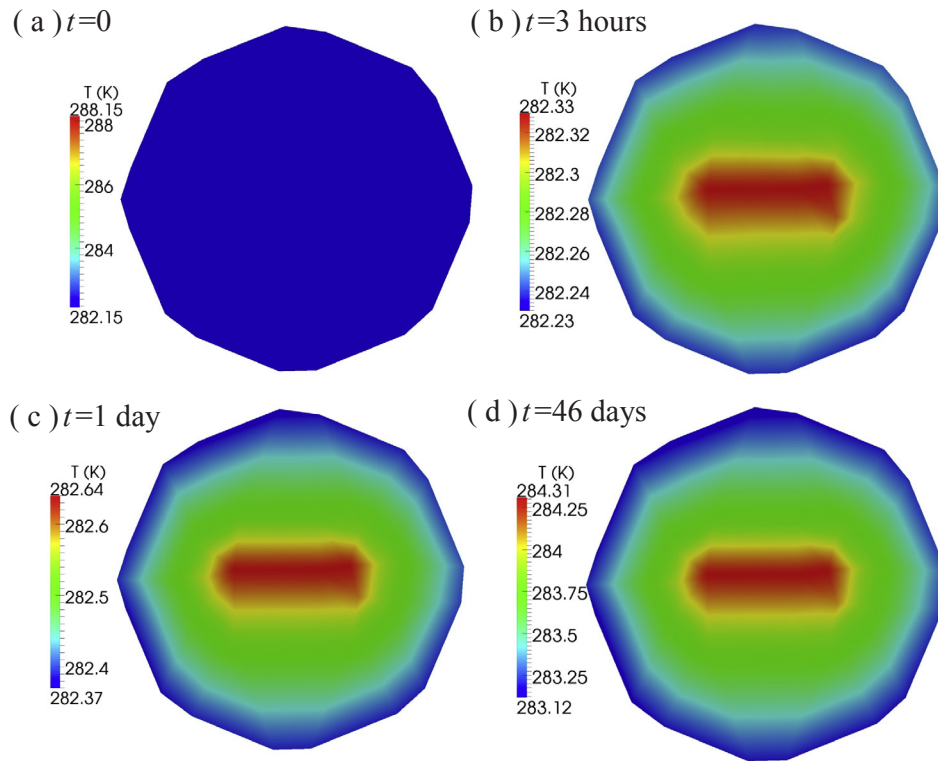


Fig. 10. Temperature contours in cross-sections at the top of the water body at different times.

distributions along depth at different times in Fig. 13b also help explain the flow patterns observed in Figs. 7 and 8 and the temperature variations in Figs. 10–12. The difference between the temperatures at  $z = 0$  m and  $z = -1159.2$  m decreases from 6 K to 2.5 K as time elapses, which is also similar to what we observed in Figs. 10–12. The mine water is mixed because its temperatures tend to gradually

approach a constant due to the natural convection. This good mixing condition is consistent with most field observations in flooded mines [18].

The circulation of the mine water due to the natural convection (Figs. 7 and 8) essentially mixes the water and significantly speeds up the heat transfer in the water. For the case shown in Fig. 13, the

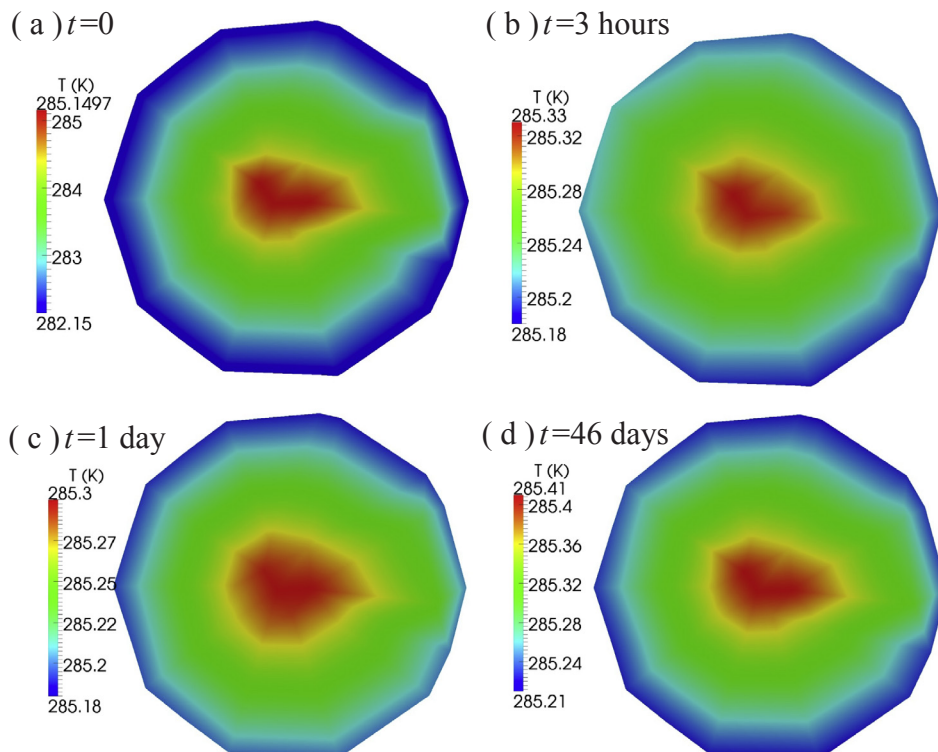


Fig. 11. Temperature contours in cross-sections in the middle of the water body at different times.

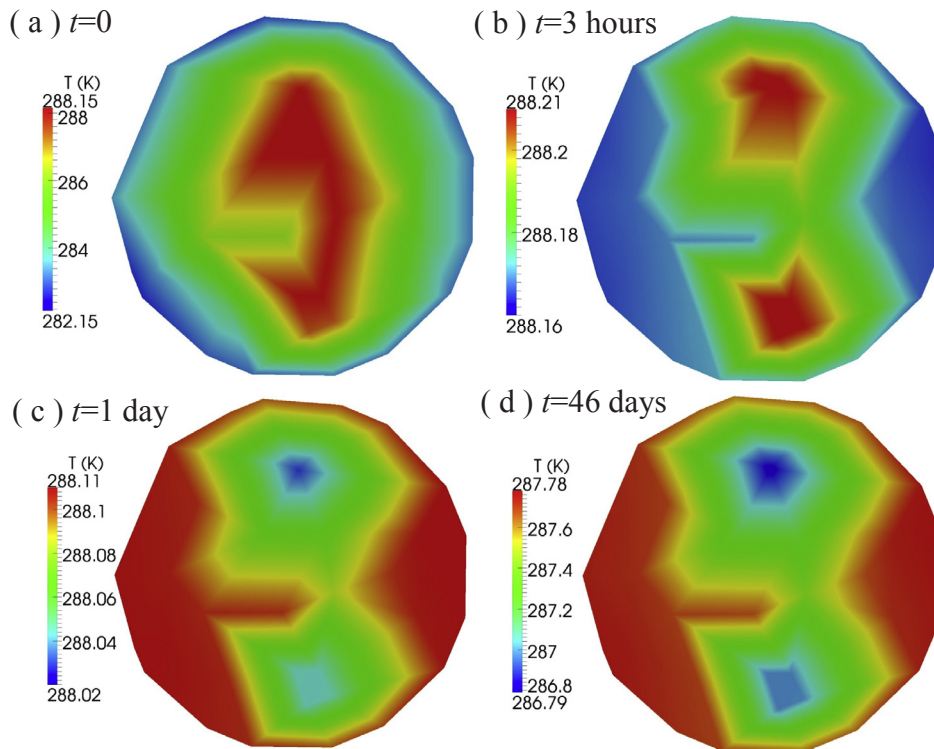


Fig. 12. Temperature contours in cross-sections at the bottom of the water body at different times.

temperatures of the whole water body in the shaft will approach an equilibrium value, making all the water in this shaft appear as one layer (cell). The mechanism inferred from the above simulation well explains the mixing of the mine water within each stratified layer in the field study, in which the temperature and chemical concentrations are approximately constant. These simulation results serve as a rough assessment to validate the buoyancy-driven flow in the mine water, which include complicated geologic conditions for the first time. It is worthwhile to mention that the influence of the intrusion through the connected drifts from adjacent mines was not considered. Therefore, further research is needed to investigate such an influence. In addition, the phenomenon regarding the mine water stratification observed in Fig. 2

was not successfully simulated in this preliminary case. One possible reason is that other factors were not included, e.g., salinity influences the density of the mine water and complicated underground mine geometries (such as drifts and fissures) affect mine water flow directions, which require much more fluid dynamics studies far beyond the scope of the current study. Therefore, future work is needed to understand the mechanisms underlying the layering phenomenon. Based on the understanding of stratification, strategies of heat extraction, e.g., target temperature layer and location of pumping pipes, can be investigated to optimize this geothermal application. Despite the above limitations, such a preliminary assessment has succeeded in reproducing the major mechanisms explaining heat and mass transfer in the

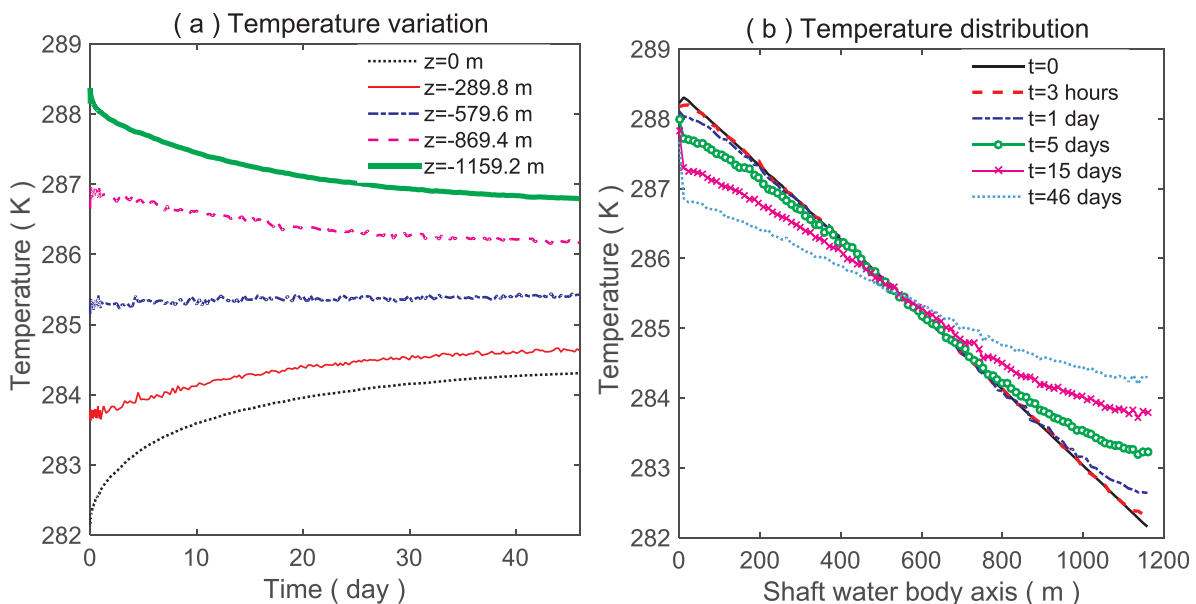


Fig. 13. Computed temperatures: (a) temperature variation at different positions, and (b) temperature distribution along the shaft water body.

complicated multiphysical processes and shedding light on what we observed from the field study.

## 5. Conclusions

This study introduces the results on the scientific understanding of the natural mine water-geologic formation system, especially the transport of heat and mass in this large-scale natural system, for exploring the water from deep abandoned copper mines as a geothermal energy resource in the U.P. of Michigan, a historical copper mining area in the U.S. Three essential components for understanding the physical processes involved in the geothermal application of the mine water were introduced: a field study, a theoretical framework, and numerical simulations. The field study yielded measurements of temperatures, electrical conductivity, and chemical concentrations in a local mine shaft in the U.P. The main purpose is to understand the key scientific issue in the use of the mine water as a geothermal resource, i.e., the temperature distribution in the mine water. The theoretical framework development provided a mathematical description for the thermo-hydrodynamic process in the mine water coupled with the heat transfer in the surrounding geologic formations for studying the scientific issue. Simulations were conducted to preliminarily investigate the quasi-equilibrium water movement in the mine shaft due to geothermal gradients to shed light on the phenomena observed in the field study.

The simulation based on the proposed framework provided explanations to the data obtained in the field from a scientific perspective, which is of practical meaning to the success of this energy renovation with water in deep flooded mines. No research is reported prior to the current study to include the comprehensive information as detailed in this study. This study fills this gap with simulations accompanied by field studies on the same deep flooded mine shaft, a pioneering one in the United States. Also, a theoretical framework for the mine water-surrounding geologic formation system has been successfully implemented to test a realistic case. Serving as a solid cornerstone, this study will be further continued for a scientific understanding to help predict the efficiency and sustainability of the energy exploration from abandoned and flooded mines using the mine water as a safe, green, relatively renewable and adaptable geothermal resource.

## Acknowledgment

The authors are grateful to Dr. Allan M. Johnson for the loan of deep water sampling equipment and mine map information and to the Keweenaw Digital Archives for the help with identifying geological and mine map information. We also acknowledge the support from the Vice President of Research Office at Michigan Tech via the Research Excellence Fund and the support from the Superior Computer Cluster for high-performance computing.

## References

- [1] Jessop AM, MacDonald JK, Spence H. Clean energy from abandoned mines at Springhill, Nova Scotia. *Energy Sour* 1995;17:93–106.
- [2] Zheng W, Ye T, You S, Zhang H. The thermal performance of seawater-source heat pump systems in areas of severe cold during winter. *Energy Convers Manage* 2015;90:166–74.
- [3] ASHRAE. *Fundamentals handbook-American society of heating, refrigerating and air-conditioning engineers*. Atlanta (GA, USA): ASHRAE; 2009.
- [4] Raymond J, Therrien R, Hassani F. Overview of geothermal energy resources in Québec (Canada) mining environments. In: 10th International Mine Water Association Congress: mine water and the environment. Ostrava (Czech Republic): Technical University of Ostrava; 2008. p. 1–12.
- [5] Malolepszy Z, Demollin-Schneiders E, Bowers D. Potential use of geothermal mine waters in Europe. In: *Proceedings of the world geothermal congress, Antalya, Turkey*; 2005. p. 1–3.
- [6] Behrooz BS, Elianne D, Jan-Jaap VB. Geothermal use of deep flooded mines. In: *International symposium on post-mining, Nancy, France*; 2008. p. 1–10.
- [7] Limanskiy A, Vasilyeva M. Using of low-grade heat mine water as a renewable source of energy in coal-mining regions. *Ecol Eng* 2016;91:41–3.
- [8] Ramos EP, Falcone G. Recovery of the geothermal energy stored in abandoned mines. *Clean energy systems in the subsurface: production, storage and conversion*. Goslar (Germany): Springer; 2013. p. 143–55.
- [9] Burnside N, Banks D, Boyce A. Sustainability of thermal energy production at the flooded mine workings of the former Caphouse Colliery, Yorkshire, United Kingdom. *Int J Coal Geol* 2016;164:85–91.
- [10] Burnside N, Banks D, Boyce A, Athresh A. Hydrochemistry and stable isotopes as tools for understanding the sustainability of minewater geothermal energy production from a ‘standing column’ heat pump system: Markham Colliery, Bolsover, Derbyshire, UK. *Int J Coal Geol* 2016;165:223–30.
- [11] Reichart G, Vaute L, Collon-Drouaillet P, Buès MA. Modelling heat and salinity related convective processes in deep mining flooded wells. In: 11th International mine water association congress, Aachen, Germany; 2011. p. 183–7.
- [12] Hamm V, Sabet BB. Modelling of fluid flow and heat transfer to assess the geothermal potential of a flooded coal mine in Lorraine, France. *Geothermics* 2010;39:177–86.
- [13] Streb C, Wieber G. Geothermal energy from a flooded mine: a hydraulic model. In: Rüdte RT, Freund A, Wolkersdorfer Ch, editors. *Mine water-managing the challenges, IMWA*; 2011. p. 189–93.
- [14] Arias CA, Alonso AO, García RÁ. Hydrogeological and thermal modelling of an underground mining reservoir. *Mathematics of planet earth*. Springer; 2014. p. 419–23.
- [15] Jessop A. Geothermal energy from old mines at Springhill, Nova Scotia, Canada; 1995. p. 463–8.
- [16] Renz A, Rühaak W, Schätzl P, Diersch H. Numerical modeling of geothermal use of mine water: challenges and examples. *Mine Water Environ* 2009;28:2–14.
- [17] Kories H, Rüterkamp P, Sippel M. Field and numerical studies of water stratification in flooded shafts. In: *Proceedings international mine water association symposium, Newcastle upon Tyne, UK*; 2004. p. 149–59.
- [18] Wolkersdorfer C. *Water management at abandoned flooded underground mines: fundamentals, tracer tests, modelling, water treatment*. München (Germany): Springer Science & Business Media; 2008.
- [19] Malolepszy Z. Low temperature, man-made geothermal reservoirs in abandoned workings of underground mines. In: *Proceedings of the 28th workshop on geothermal reservoir engineering, Stanford, California, USA*; 2003. p. 259–65.
- [20] Hamm V, Collon-Drouaillet P, Fabriol R. Two modelling approaches to water-quality simulation in a flooded iron-ore mine (Saizerais, Lorraine, France): a semi-distributed chemical reactor model and a physically based distributed reactive transport pipe network model. *J Contam Hydrol* 2008;96:97–112.
- [21] Clark RR. A new continuous-sampling wireline system for acquisition of uncontaminated, minimally disturbed soil samples. *Groundwater Monit Remediat* 1988;8:66–72.
- [22] Dines C, Cowan P, Headworth C. An operational subsea wireline system. In: *SPE offshore South East Asia conference and exhibition, Singapore*; 1988.
- [23] Piatak NM, Seal RR, Hammarstrom JM, Kiah RG, Deacon JR, Adams M, et al. Geochemical characterization of mine waste, mine drainage, and stream sediments at the Pike Hill copper mine superfund site, Orange County, Vermont. Reston (Virginia): U.S. Environmental Protection Agency U.S. Geological Survey; 2006. p. 1–131.
- [24] Kubitz J, Lewek E, Besser J, Drake J, Giesy JP. Effects of copper-contaminated sediments on *Hyalella azteca*, *Daphnia magna*, and *Ceriodaphnia dubia*: survival, growth, and enzyme inhibition. *Arch Environ Contam Toxicol* 1995;29:97–103.
- [25] Liu Z, Yu X. Coupled thermo-hydro-mechanical model for porous materials under frost action: theory and implementation. *Acta Geotech* 2011;6:51–65.
- [26] Liu Z, Yu XB, Tao J, Sun Y. Multiphysics extension to physically based analyses of pipes with emphasis on frost actions. *J Zhejiang Univ Sci A* 2012;13:877–87.
- [27] Robertson EC. *Thermal properties of rocks*. Reston (Virginia): US Geological Survey; 1988. p. 1–110.
- [28] Butler BS, Burbank WS. *The copper deposits of Michigan*. US Government Printing Office; 1929.
- [29] Oliveira PJ, Issa RI. An improved PISO algorithm for the computation of buoyancy-driven flows. *Numer Heat Transf Part B: Fundam* 2001;40:473–93.
- [30] Ferziger JH, Peric M. *Computational methods for fluid dynamics*. Springer Science & Business Media; 2012.
- [31] Bao T, Liu Z. Large-scale thermo-hydrodynamic modeling of a flooded underground mine for geothermal applications. *Geo-Chicago* 2016. ASCE; 2016. p. 72–83.
- [32] Schön JH. *Physical properties of rocks: fundamentals and principles of petrophysics*. Elsevier; 2015.
- [33] Manger GE. *Porosity and bulk density of sedimentary rocks*. Washington: Geological Survey Bulletin; 1963. p. 1–60.